Lithuanian Journal of Physics
Vol. **66**, No. 2, pp. 91–106 (2026)
ISSN 1648-8504 eISSN 2424-3647
DOI: https://doi.org/10.3952/physics.2026.66.2.4

INFLUENCE OF Fe^{2+} ON LIPID ORIENTATION IN THE CELL MEMBRANE BILAYER: QUANTUM CHEMICAL MODELLING

T. Kondrotaitė-Intė [a, b], A. Gruodis [c], and G. Saulis [b]

[a] *Department of Mechanical and Materials Engineering, Vilnius Gediminas Technical University, Plytinės 25, 10105 Vilnius, Lithuania*

[b] *Department of Biology, Faculty of Natural Sciences, Vytautas Magnus University, Universiteto 10-314, Akademija,* 53361 *Kaunas, Lithuania*

[c] *Institute of Chemical Physics, Vilnius University, Saulėtekio 3, 10257 Vilnius, Lithuania*

Email: alytis.gruodis@ff.vu.lt; gintautas.saulis@vdu.lt; terese.kondrotaite@gmail.com

Received 29 December 2025; accepted 21 January 2026

To understand the dynamics of hole formation and the progression of hole closure in the membrane layer at the molecular level, the structures of phospholipids and iron-ion associates were modelled using quantum-mechanical methods. It has been found that metal ion fixation to the lipid chain is insignificant in forming lipid conformational movement. Similarly, metal ion fixation in the case of the $-N(CH_3)_3$ head in the lipid head group is not formed. The iron ion binds two lipid molecules in the orthophosphoric region, forming an energetically stable bridge between orthophosphoric fragments. As a result of this process, the lipid aliphatic chains change their conformation: a curved chain forms around the metal ion centre from a straight structure. A typical molecular charge redistribution during excitation was determined and described. It is stated that, due to the energetically favourable position of the Fe^{2+} ion, one lipid serves as a charge donor and the other as a charge acceptor.

Keywords: Fe^{2+} ion, phospholipids, lipid–Fe–lipid associate, complex stability

1. Introduction

Phospholipids are the main structural components of biological membranes, playing a crucial role in the formation, maintenance and alteration of labile changes, and in the transmission of barrier-layer functions [1, 2]. Lipids serve as the primary constituents of the cell membrane, playing a crucial role in maintaining its structure and regulating cellular functions [3]. Glycerol-based phospholipids, which are the main components of biomembrane, are amphiphilic molecules characterized by their hydrophobic tails and hydrophilic head groups [4]. The head group can possess a charge, whether positive or negative, or it may remain neutral [5]. In an aqueous environment, lipids assemble into a lipid bilayer because of hydrophobic interactions [6]. Typically, lipid tails consist of one saturated fatty acid chain and one unsaturated fatty acid chain, leading to the formation of 'liquid crystal' membranes [7].

The bilayer may exist in various states, including liquid, gel, resistance, or pulsating phase [8–10]. Phospholipids exhibit variations in their melting temperatures, influencing the melting behaviour of neighbouring lipids [11]. Within a single lipid bilayer, multiple phases can coexist at identical temperature and pressure, influenced by varying compositions [12]. The geometric shape of the phospholipids determines the preferred membrane curvature for them [13]. Natural phospholipids typically possess two tails and exhibit an almost cylindrical shape, resulting in the formation of a straight bilayer [14]. However, certain lipids exhibit a propensity to create significant bends, such as cardiolipin, characterized by its four tails, or lysoPC, which possesses a single tail [15]. The physical state of membrane lipids

plays a crucial role, as these lipids can influence the physiological condition of membrane organelles by modifying their biophysical properties, including polarity and permeability [16].

Under standard physiological conditions, direct permeability through the membrane without external exposure is limited. Induced effects from outside (uncontrolled discharge of electricity, electroporation, formation of acidic, alkaline media, localization of aggressive metal ions) allow cell membrane damage through lipid conformational and destructive processes [17–19]. Such an invasive cell assay method as electroporation is increasingly used for the testing of the cell composition [20]. However, unknown side processes during electropore generation can greatly impair the result of cell manipulation if uncontrolled factors change the course of the experiment [21].

Electroporation is a process in which cells or tissues are subjected to strong electric-field pulses, leading to a temporary increase in cell membrane permeability due to the formation of aqueous pores within the lipid bilayer [22]. Under suitable conditions, cell viability can be maintained. For this reason, electroporation is used in molecular biology, biotechnology and medicine as a method for delivering selected small molecules into cells [23]. The initiation of pore formation occurs when the transmembrane potential of several hundred mV is established across the lipid membrane. The threshold for electroporation depends on the lipid bilayer composition [24]. It is known that enhancing the transmembrane potential through the application of an electric field facilitates the creation of pores within the lipid bilayer [25]. Studies in molecular dynamics have demonstrated that in sufficiently large systems pores of up to 10 nm can form independently [26]. The model demonstrated that the electroporation process comprises two distinct stages. Initially, water molecules establish a chain-like configuration and infiltrate the hydrophobic membrane layer. This penetration occurs more readily in regions where lipid head groups exhibit local imperfections. Secondly, chains of water molecules grow and expand, forming aqueous pores. The charge of the lipid head group and the solution of the cellular environment do not influence electroporation [26].

Nonetheless, electro-induced pores fail to explain a molecular mechanism that accounts for the prolonged cell membrane permeability, which can persist for several hours following exposure to the pulse [27]. The closure time is significantly longer than the electroporation closure time determined through molecular dynamics simulation studies [28]. Experimental studies suggest that lipid peroxidation may explain the mechanism behind the extended membrane permeability [29–32].

Oxidative stress is an inevitable consequence of living in an oxygen-enriched atmosphere. As a secondary product of the aerobic metabolism, induced by various natural and synthetic toxic substances, oxygen radicals and other activated forms of oxygen are produced [33]. To protect against cell damage, the organism has several levels of antioxidant protection, repair and renewal mechanisms [34]. Oxidative stress occurs when the prooxidant–antioxidant system is disrupted, and the organism is no longer able to protect itself from oxidative effects [35]. Lipid peroxidation occurs when reactive oxygen species, including free radicals, oxidize lipids that contain double bonds, especially polyunsaturated fatty acids, leading to the disruption of a membrane structure and function [36, 37]. This process is believed to be associated with diseases such as Parkinson's, Alzheimer's, schizophrenia, atherosclerosis, inflammatory diseases, cancer, diabetes, damage to the heart ischemic reperfusion, and cell aging [38].

Biologically, lipid peroxidation can occur through enzymatic mediation or through non-enzymatic processes [39]. Enzymatic lipid peroxidation, primarily facilitated by cyclooxygenases, lipoxygenases and cytochrome P450, results in the formation of lipid hydroperoxides, which are generally reduced by glutathione peroxidase. However, when this detoxification process is either overwhelmed or compromised (for instance, by 4-hydroxynonenal), hydroperoxides can accumulate and contribute to non-enzymatic lipid peroxidation through radical chain reactions [40, 41]. Within cellular environments, these reactions may be initiated by reactive species produced internally, such as those from mitochondrial electron transport and radical-generating enzymes like NADPH oxidase or they can be triggered by external stressors, including ultraviolet or ionizing radiation and various environmental chemicals, while *in vitro*, these reactions are frequently induced by transition metals like iron and copper, as

well as hydroxyl radicals or irradiation [42]. Historically, a phenomenon involving the reaction of molecular oxygen and lipids through a free radical chain reaction is referred to as autoxidation [43]. Primary products of autoxidation are peroxides or hydroperoxides, but often these compounds are unstable and degrade to aldehydes, ketones, and other reactive structures [44]. The mechanism of lipid peroxidation can be characterized by three phases: initiation, propagation and termination – see Fig. 1.

During the initiation phase, a radical compound is generated from non-radical molecules. This is accomplished in cells through the utilization of iron, with copper being used less frequently. Cellular iron regulation is highly controlled, with extracellular iron bound to transferrin and over 95% of intracellular iron associated with proteins, resulting in only a minimal labile pool available for involvement in redox reactions [45]. The initial phase involves the Fenton reaction, which was first detailed by Fenton in 1890s [46, 47]:

$$Fe^{2+} + HO–OH \rightarrow Fe^{3+} + {}^{\bullet}OH + HO^{-}, \quad (1)$$

$$Fe^{3+} + HO–OH \rightarrow Fe^{2+} + {}^{\bullet}OOH + H^{+}. \quad (2)$$

Ferrous iron (Fe^{2+}) reacts with hydrogen peroxide, forming ferric iron (Fe^{3+}) and highly reactive radicals. When excess peroxide is present, Fe^{3+} can be converted back to Fe^{2+}. However, this redox cycling is more favourable at low pH levels and is constrained under aerobic conditions due to the rapid oxidation of Fe^{2+} and the precipitation of Fe^{3+} as $Fe(OH)_3$ [48]. Lipid peroxidation is most effective at a Fe^{2+}:Fe^{3+} ratio of approximately 1:1 to 1:2, with increased levels of Fe^{3+} leading to a reduction in the lag phase following oxygen uptake [49]. Propagation involves hydroxyl and peroxyl radicals abstracting hydrogen from unsaturated membrane lipids, leading to the formation of carbon-centred radicals. These radicals then react with O_2 to generate lipid peroxyl radicals (LOO•), which subsequently produce lipid hydroperoxides (LOOH) while also regenerating radicals, thus sustaining a chain reaction. During the termination stage, when the radical concentration reaches a level sufficient for interaction, they engage in a reaction that forms new bonds, thereby eliminating the radicals. Similarly, antioxidant molecules [41], which can donate electrons without themselves becoming radicals, can halt radical scattering.

Both saturated and unsaturated phosphatidylserines exhibit a similar resistance to iron-driven lipid peroxidation. This is likely due to the phosphatidylserine head group's ability to chelate iron, thereby reducing the availability of free redox-active ions. In contrast, other lipid head groups bind iron less effectively, resulting in a minimal inhibition [50]. Tang et al. (2000) found that the elimination of pre-oxidized membrane lipids halted both the initiation of lipid peroxidation and the oxidation of Fe^{2+}. This indicates that the presence of pre-existing lipid hydroperoxides and lipid peroxyl radicals might be essential for initiating Fe^{2+}-driven peroxidation, thereby explaining the observed lag phase, critical Fe^{2+} ratio, and the dependence on Fe^{2+} oxidation [51].

Reactive lipid forms produced through either pathway exhibit electrophilic properties and engage with cellular nucleophiles, such as cysteine, lysine and histidine amino acids [52]. Reactive lipid forms have been found to be involved in several physiological processes, including pre-inflammatory reactions, programmed cell death, and induction of cellular antioxidants by modification of specific signalling proteins [53].

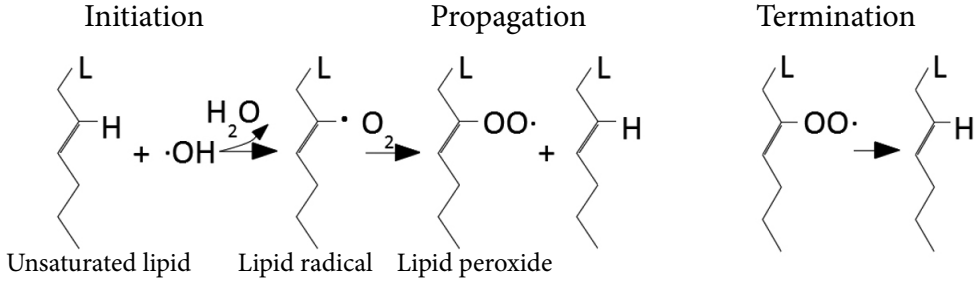

Fig. 1. Scheme of the chain lipid peroxidation reaction.

Therefore, it is necessary to understand the molecular-level dynamics of hole formation and closure in the membrane layer. Since the membrane is a lipid bilayer, it is necessary to evaluate not only the physical but also the chemical aspects: redox reactions in the near environment generate many ionized species that essentially catalyze the aforementioned factors. Metal ions belong to these factors. This work is devoted to the systematic structural analysis of molecular associates of orthophospholipids with Fe^{2+} ions in the case of the lowest electronic excitations using density functional simulations.

2. Materials and methods

2.1. Methodology

Molecular mechanics methods approximate the energy surfaces of quantum mechanics by classical mechanics models. However, it is only suitable for modelling the most probable structures since these methods only compare different configurations of the molecule, but do not consider the electronic properties [54]. Semi-empirical methods are based on quantum-physical models that use empirical parameters from experiments to parameterize two-electron integrals. These methods are surprisingly effective for calculating the electronic absorption spectrum and jump-state parameters. They are applicable to small-molecule systems with π-conjugated systems [55].

2.2. Object of modelling

The object of modelling is an orthophospholipid composed of an aliphatic chain, an orthophosphorous group and an amino group. 2-Decenoic acid and decanoic acid (Fig. 2), as well as 3-decenoic acid and decanoic acid, were selected as the aliphatic chain group of the analogous lipid to reduce the computation time. 2-Decenoic and 3-decenoic acids were chosen for the aliphatic unsaturated fatty acid chain, as the lower-state energy estimates of the cis and trans conformational structures of the decene structures show that 2-decenoic and 3-decenoic acids have lower state energy than other decenoic acids.

Phospholipid structure modelling was performed when Fe^{2+} ion interacts

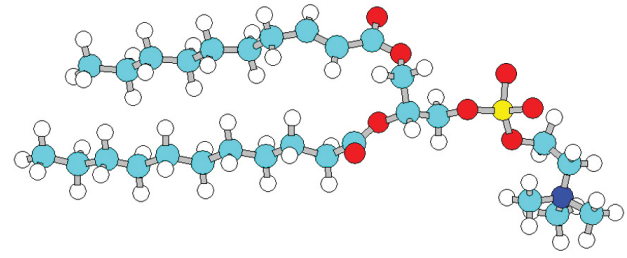

Fig. 2. The object of modelling – glycerol-phospholipid whose unsaturated fatty acid chain consists of 2-decenoic acid fragments.

a) with a lipid head [$–NH_3$] or [$–N(Me)_3$];
b) with a lipid aliphatic chain (full and truncated);
c) with a lipid orthophosphoric group.

2.3. Simulation

Optimization of associate geometry was performed by the Gaussian 16 [56] program, using the semi-empirical density function method B3LYP by means of the Gaussian basis set 6-31G. The influence of the solvent media (water) was evaluated by the polarized continuum model (PCM) [57].

3. Results

3.1. Interaction of Fe^{2+} ion with the lipid aliphatic chain and lipid $–NH_3$ head

To evaluate the energy properties of phospholipid derivatives under the influence of the medium, the interactions of metal ions, hydroxyl radicals, and anions with phospholipid tail and head groups were investigated using molecular geometry optimizations by the density functional method, including solvent enclosure.

To investigate the influence of metal ions and hydroxyl radicals and anions on the lipid aliphatic chain group, several structures (containing Fe^{2+} ions only as well as Fe^{2+} ions together with the hydroxyl anions and radicals) were modelled. Neither lipid peroxidation initiation nor Fe^{2+} oxidation was observed (Fig. [3]). The metal ion and hydroxyl radical charges and energy are too weak to separate hydrogen from the membrane unsaturated fatty acid. Therefore, no conformational and energetic structural changes were observed. This phenomenon does not rule out the theory put forward by Tang and colleagues that to initiate lipid peroxidation

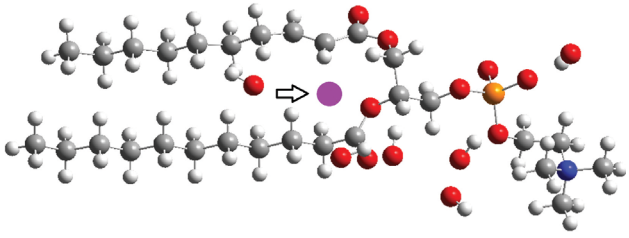

Fig. 3. Associate of Fe^{2+} ion (in violet colour, shown by an arrow) with hydroxyl radicals and ortho-phospholipid.

Fe^{2+} (and other metals) ions and active oxygen forms alone are not sufficient; the cell must be pre-LOOH and LOO• groups [51].

To find the influence of Fe^{2+} in the lipid medium on the lipid head group, the Fe^{2+} ion was placed between the two lipid head groups (Fig. 4). When it was observed that the interaction of Fe^{2+} ion with the lipid head does not affect the lipid tail group (Fig. 4), in order to shorten the computation and optimization time, the aliphatic chains in the lipid tail group were replaced with propanoic acids.

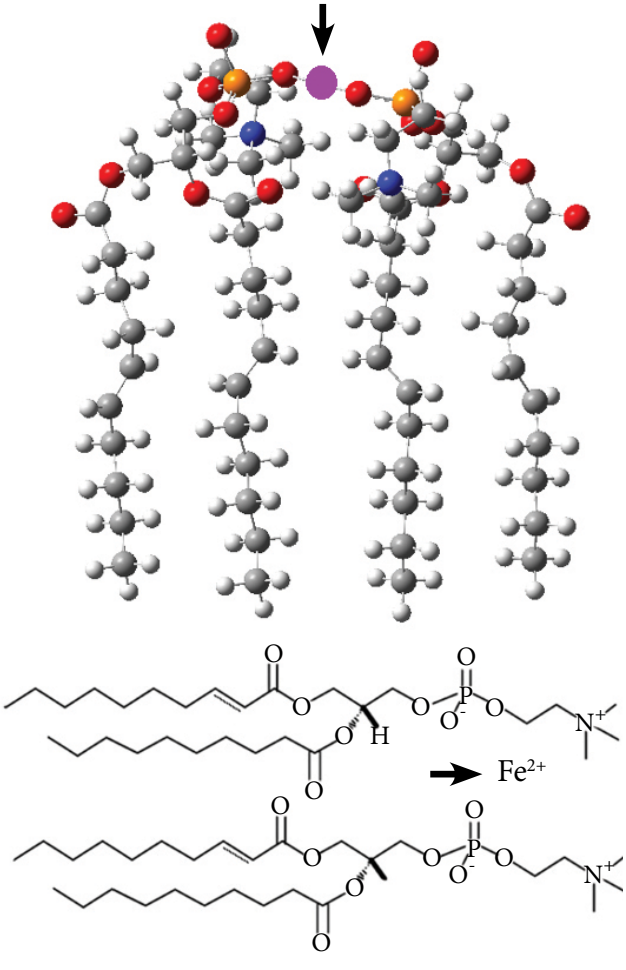

Fig. 4. An associate of Fe^{2+} ion (in violet colour, shown by an arrow) and two ortophospholipids.

After performing the usual geometry optimization procedures, it was concluded that the fixation of Fe^{2+} ions with the [–NH_3] or [–NMe_3] head does not occur in the region of phospholipid head groups, and a sufficiently stable association or complex (as in the case of a physical dimer) is not formed – see Fig. 4. A stable bridge between the two lipids in the head region, containing metal ions, practically does not exist. A similar situation is also found in the region of the [–C=C–] fragment of the aliphatic chain, where there is no possibility at all for the formation of a stable [>Fe^{2+}<] bridge.

3.2. Interaction of a Fe^{2+} ion with an orthophosphoric fragment of lipid

The Fe^{2+} ion aggregates with lipids in the orthophosphoric region, forming a metal bridge for the associate of the lipid–Fe–lipid type. This coupling initiates a conformational process – related with the rotations of [–NMe_3] heads. It can be assumed that when the phospholipids bind the Fe^{2+} ion in the orthophosphoric region, the lipid aliphatic chain also changes the position substantially. A linear conformation (such as Fig. 7 or Fig. 9) was chosen to model the structure of the lipid chain. The Fe^{2+} ion was placed at the orthophosphoric group at a distance of >0.5 nm from the oxygen atoms (in comparison, the [–C–C–] bond corresponds to 0.153 nm).

After preparation of several initial structures, the optimal geometry of the lipid–Fe–lipid associate was simulated using the density functional B3LYP method and the 6-31G (d) basis set with polarizing d functions. Three most interesting associates (Table 1) are discussed here. For these three structures, the optimization problem was solved completely, and the four convergence values obtained are in satisfactory ranges. For the structures D1, D2 and D3, the binding energy was calculated as the difference between the sum of the energies of the individual two lipids and the metal ion with two protons and the energy of the associate. The formation of the Fe^{2+} bridge takes place at different positions of the Fe^{2+} ion and lipids. It can be assumed that when the Fe^{2+} ion enters the orthophosphoric region of the phospholipid head group, this bridge

will always form. It should be noted that the influence of the solvent was not included in the calculation of the binding energy (Table 1), and a poorer base was used. For this reason, the received binding energy is significantly higher than the experimentally observed value. According to Durrant [58], the formation of the [–Fe–O–] bonded dimer is more favourable by –17.0 kcal mol^{-1} per bond. Due to that, binding energy must exceed a value that is equal to approximately 2 eV.

Table 1 shows the structure projection scheme: each structure in the optimized geometry is presented with two projections, XOY and XOZ, to orient it based on the formed joints (Figs. 5, 7, 9). Still, the high density of atomic arrangements creates a chaotic nature, which is why only the positions of orthophosphoric and metal atoms in analogous projections are presented separately.

It should be emphasized that the formation of associates is related to the conformational processes of the aliphatic chain in the location of the metal ion.

After obtaining the structures of the optimized geometry (Figs. 5, 7, 9), the lowest electronic excitations were calculated by the semiempirical TD-DFT method.

Figure 5 depicts a D1 lipid configuration in which two phospholipid molecules are linked by an Fe^{2+} ion-mediated bridge established within the orthophosphoric region. The complementary XOY and XOZ projections offer orthogonal perspectives that enhance the visualization of the three-dimensional configuration of this complex. The formation of such a structure is determined by the interaction of the Fe^{2+} ion with the orthophosphoric group of the lipid. To enhance understanding, Fig. 5(b) focuses on this specific local binding environment, depicting the interacting orthophosphate regions in close proximity to the Fe^{2+} ion. This configuration involves Fe^{2+}

Table 1. The three most probable associates of the lipid–Fe–lipid type.

Name	Structure chart	Binding energy, eV	Binding energy, kJ/mol
D1	Fig. 5	5.21	502.7
D2	Fig. 7	4.96	478.6
D3	Fig. 9	7.79	751.7

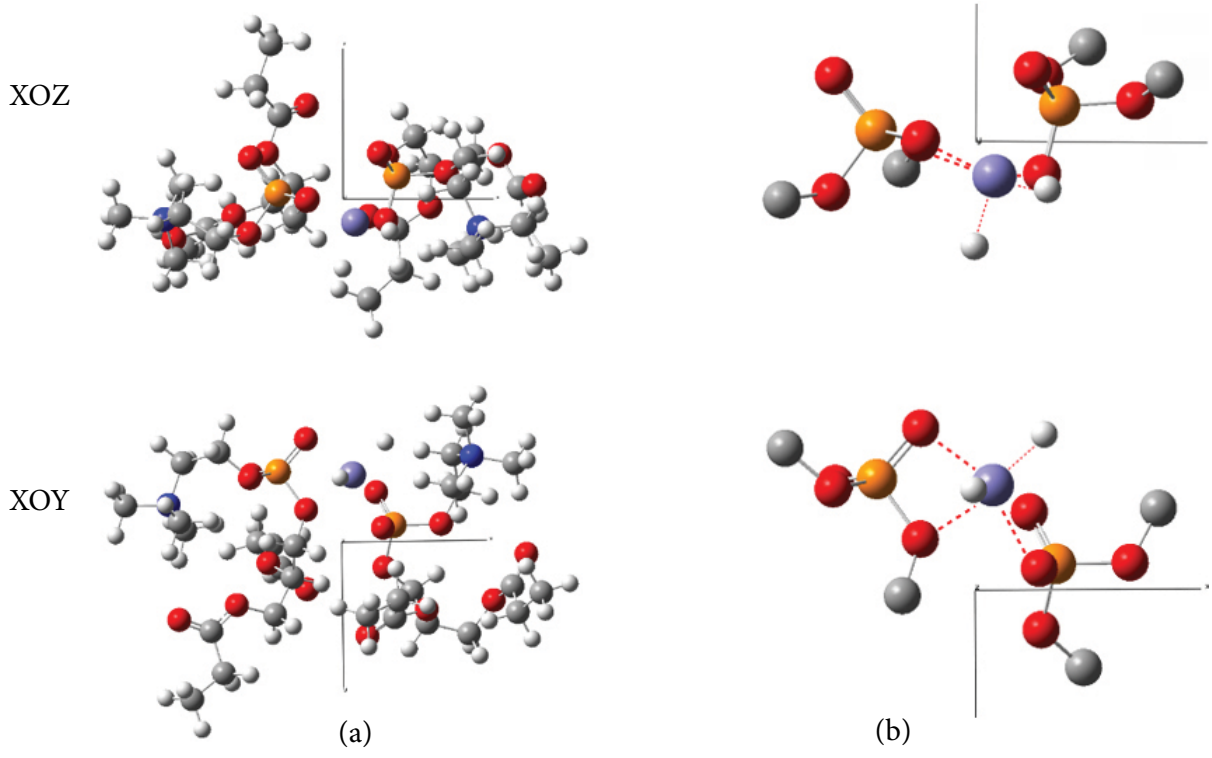

Fig. 5. D1 associate: two phospholipids related to the Fe^{2+} ion bridge (a) and the central region of the bridge bonding (b). The top and bottom represent projections XOZ and XOY, respectively.

interacting with the phosphoryl oxygen [–P=O] and the non-bridging phosphate oxygen [–P–O–] of the first lipid, along with the non-bridging phosphate oxygen [–P–O–] of the second lipid. This results in a bridged assembly stabilized by weak, non-covalent Van der Waals interactions, as represented by dotted lines.

Figure 6 illustrates the molecular orbitals of the D1 associate that participate in a forbidden electronic transition of 0.79 eV from the ground-state (MO 210, 211, 212) to the first excited state (MO 226). In the ground state, the electron density is mainly concentrated on the Fe^{2+} centre and the orthophosphate fragment, reflecting a character predominantly influenced by metal–phosphate interactions. The contributing orbitals are categorized as *d*-, *σ*-, and nonbonding (*n*) types for MO 210, 211 and 212, respectively. Upon excitation to MO 226,

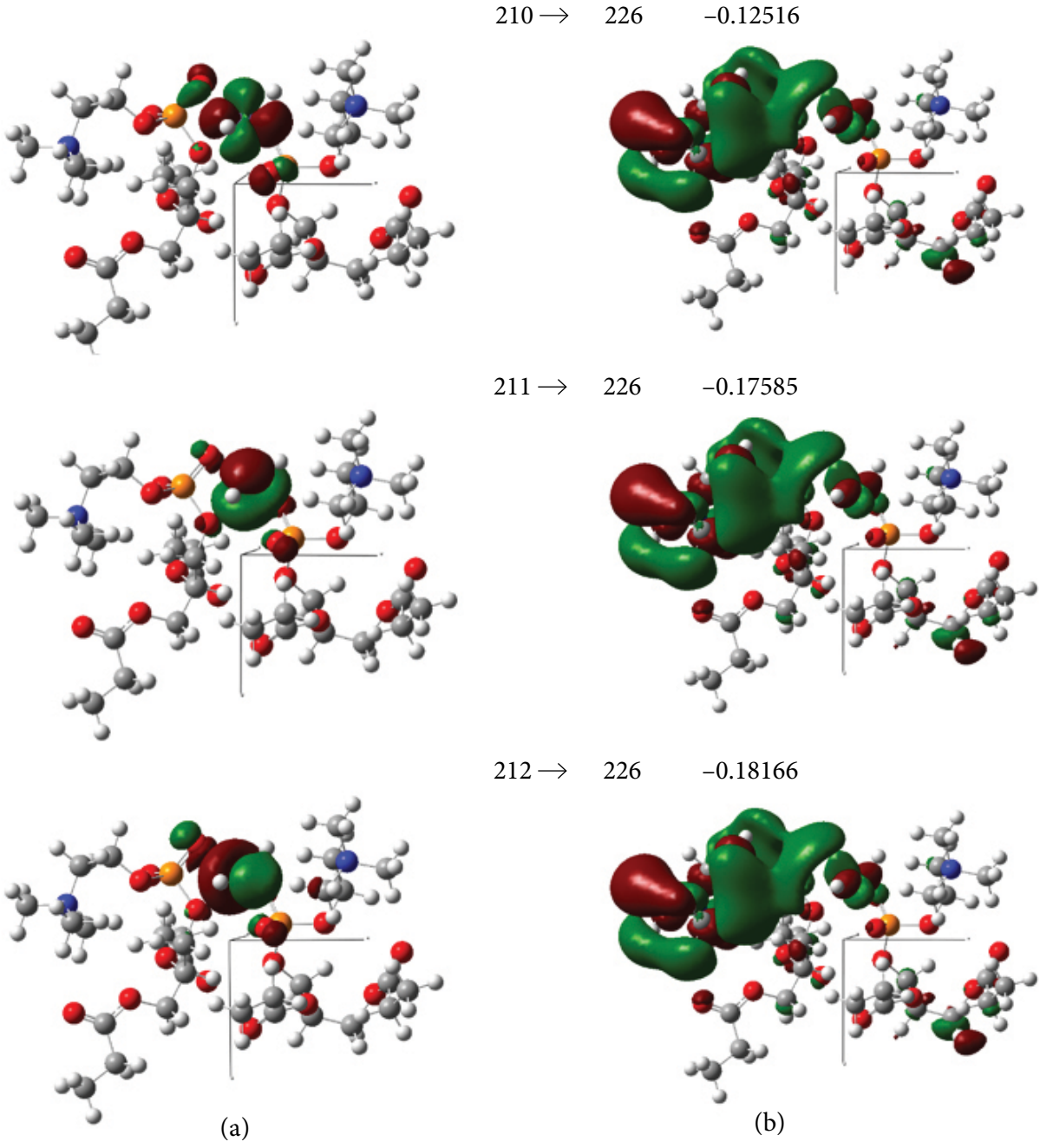

Fig. 6. Associate D1: two phospholipids bridged by Fe^{2+} ion in the orthophosphoric region, projection XOY. Molecular orbitals correspond to a forbidden electronic transition of 0.50 eV from the ground state (a) to the first excited state (b).

the presence of reactive hydrogen atoms coordinated to the metal promotes charge redistribution toward the [–NMe_3] head group of the left lipid. In this excited-state framework, the lipid on the right primarily serves as the electron donor, while the lipid on the left operates as the acceptor. The –NMe_3 head acts as an efficient relay site for charge migration, leading to the formation of a mixed σ–π bond that helps stabilize the lipid–Fe–lipid associate.

The D2 associate consists of two phospholipids linked by a Fe^{2+}-mediated bridge in the orthophosphate region, with the assembly facilitated by the coordination of the metal ion and the lipid phosphate functionalities (Fig. 7). In this arrangement, Fe^{2+} interacts with the phosphoryl group [–P=O] of the initial lipid, while also engaging with two sites on the second lipid, one non-bridging phosphate oxygen [–P–O–] and one phosphoryl oxygen [–P=O], resulting in weak, non-covalent, Van der Waals interactions represented by dotted lines. It is important to note that Fe^{2+} and the associated hydrogen ions exhibit a predominantly coplanar arrangement, resulting in a reduced interaction strength and, consequently, a weaker bonding in the bridge.

A forbidden electronic transition at 0.15 eV is observed for the D2 associate. This corresponds to the excitation from the ground state (MO 212) to the lowest excited state (MO 217, 218 and 224), as illustrated in Fig. 8. The ground-state orbital (MO 212) shows that electron density is primarily focused on the Fe^{2+}–orthophosphate interaction site, displaying a predominantly π orbital. Upon excitation to MO 217, the right lipid functions as a charge donor while the left lipid serves as a charge acceptor, resulting in partial charge density transfer to the left head group (–NH_3), where a σ-type orbital becomes evident. At the same time, charge redistribution penetrates the aliphatic tail region, resulting in a combination of σ–π orbital contributions, with the most significant localization occurring at the Fe^{2+}–orthophosphate interface, where an excited σ orbital is generated. A comparable trend is observed for MO 218; however, in this orbital, charge delocalization is more significant over

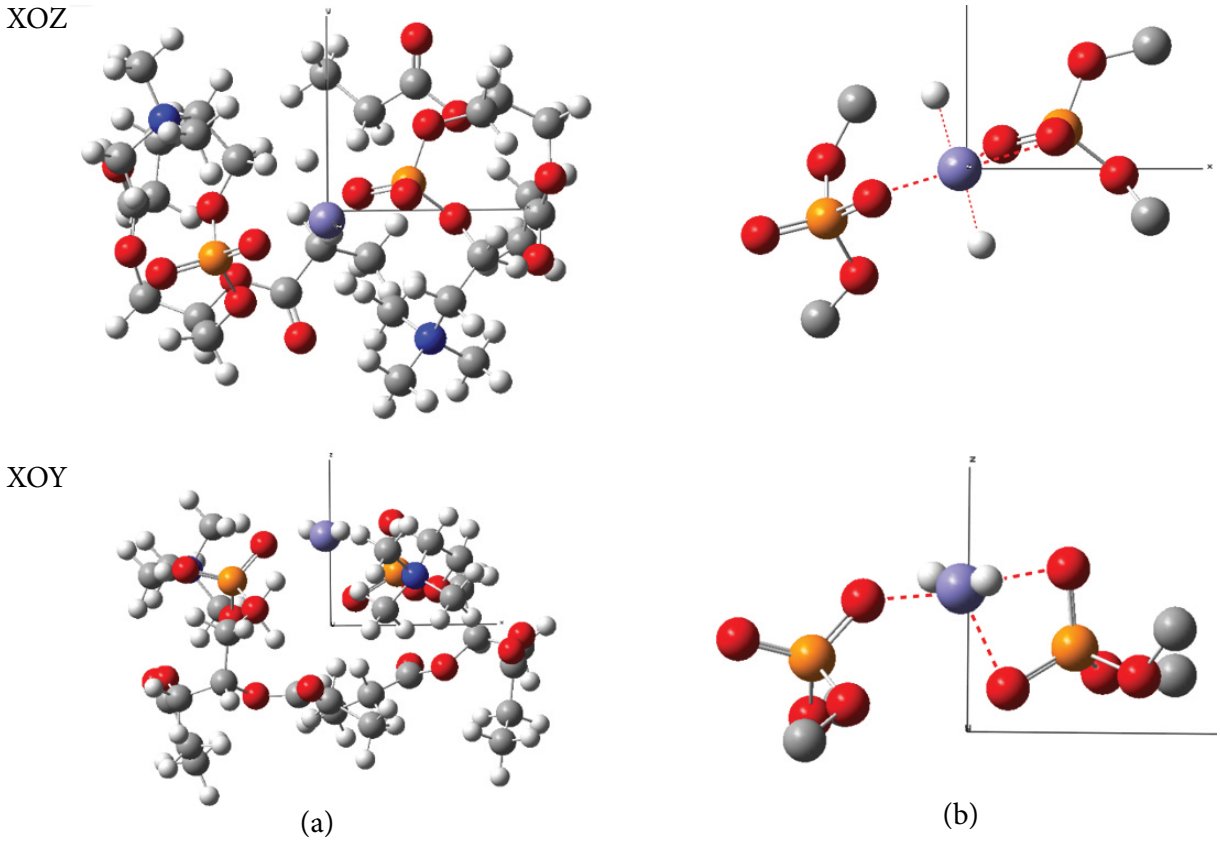

Fig. 7. D2 associate: two phospholipids related to the Fe^{2+} ion bridge in the orthophosphoric region (a) and the central region of bridge bonding (b). The top and bottom represent projections XOZ and XOY, respectively.

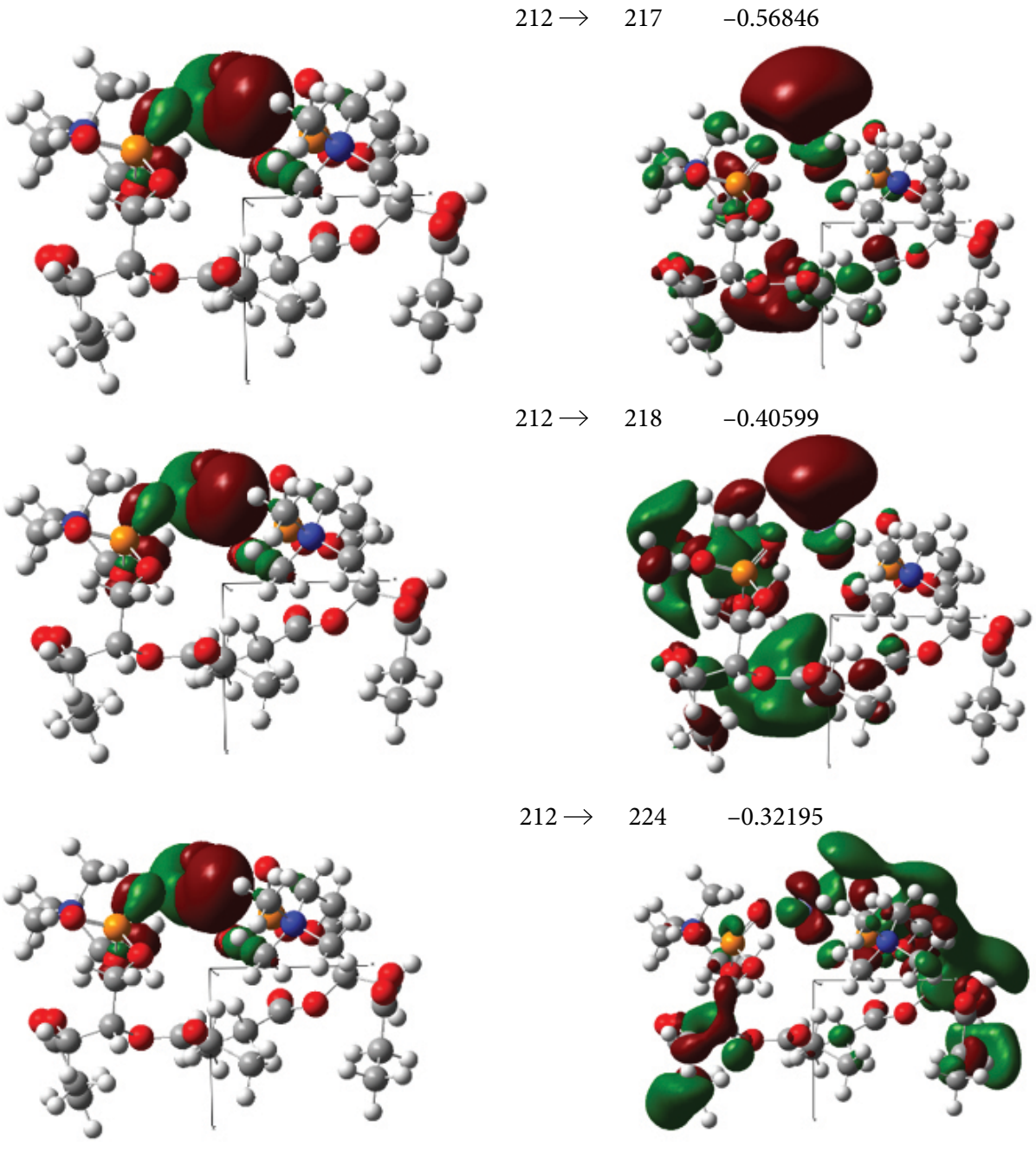

Fig. 8. D2 associate: two phospholipids bridged by Fe^{2+} ion bridge in the orthophosphoric region, projection XOZ. Molecular orbitals correspond to a forbidden electronic transition of 0.15 eV from the ground state (a) to the first excited state (b).

the left lipid [$-NMe_3$] and the tail regions, with σ–π orbital hybridization emerging as the primary stabilizing factor in these regions.

Upon excitation to MO 224, the charge transfer direction shifts in comparison to MO 217 and MO 218, with the left lipid serving as the donor and the right lipid as the acceptor. At the Fe^{2+}–orthophosphate interface, the electron density exhibits a distinct π orbit character. In this excited state, Fe^{2+} also interacts with the phosphorus centre of the right lipid, and the transferred charge is distributed as a mixed n–σ–π orbital hybrid, delocalized over the orthophosphate surface and extending into the adjacent tail region. A minor portion of charge additionally disperses along the left lipid tail, resulting in the formation of a weak σ–π

orbit hybrid. The notable engagement of the aliphatic chains suggests a distinctive redistribution pathway in which lipid tails actively contribute to charge accommodation rather than being electronically passive.

The D3 associate comprises two phospholipids linked by a Fe^{2+}-mediated bridge in the orthophosphate region, as depicted in Fig. 9. In this configuration, the metal centre interacts with two binding sites: the phosphoryl oxygen [–P=O] of the first lipid and the non-bridging phosphate oxygen [–P–O–] of the second lipid, resulting in two weak, non-covalent Van der Waals bonds represented by dotted lines. In contrast to the D1 and D2 motifs, the Fe^{2+} ion establishes a singular interaction with each lipid, rather than engaging in multiple contacts within a single head group. It is important to note that this more straightforward two-point coordination correlates with a higher binding energy than the associates previously examined (Table 1).

A forbidden electronic transition is observed at 0.37 eV for the D3 associate, indicating excitation from the ground-state π orbital (MO 212) to the first excited state (MO 220), as illustrated in Fig. 10. In MO 212, there is a notable concentration of electron density at the interface between Fe^{2+} and orthophosphate. Upon excitation to MO 220, the charge-transfer direction reveals the left lipid functioning as the donor while the right lipid acts as the acceptor. Simultaneously, the Fe^{2+}-centred π orbit transitions into a primarily mixed nonbonding–σ (n–σ) orbital. A localized redistribution pathway is established through the hydrogen atom coordinated to Fe^{2+}, directing charge toward the right lipid head group [–NMe_3], where the formation of a stabilizing σ–π hybrid orbital is evident.

Based on these findings, we suggest that the introduction of a metal ion into the orthophosphate area can create a Fe-mediated connection between neighbouring lipid head groups, leading to localized molecular distortion that aligns with the formation of pores in the bilayer. The observed conformational changes appear to be linked to an uneven charge distribution, with one lipid acting as an electron donor and the other as an acceptor. In this scenario, charge is transferred across the bridge and preferentially localizes on the opposing lipid head-group amine, with accumulation on the head group [–NMe_3] providing an additional stabilization of the lipid–Fe–lipid associate. The ongoing localization of charge at the head group would impede the re-alignment of lipids into a relaxed,

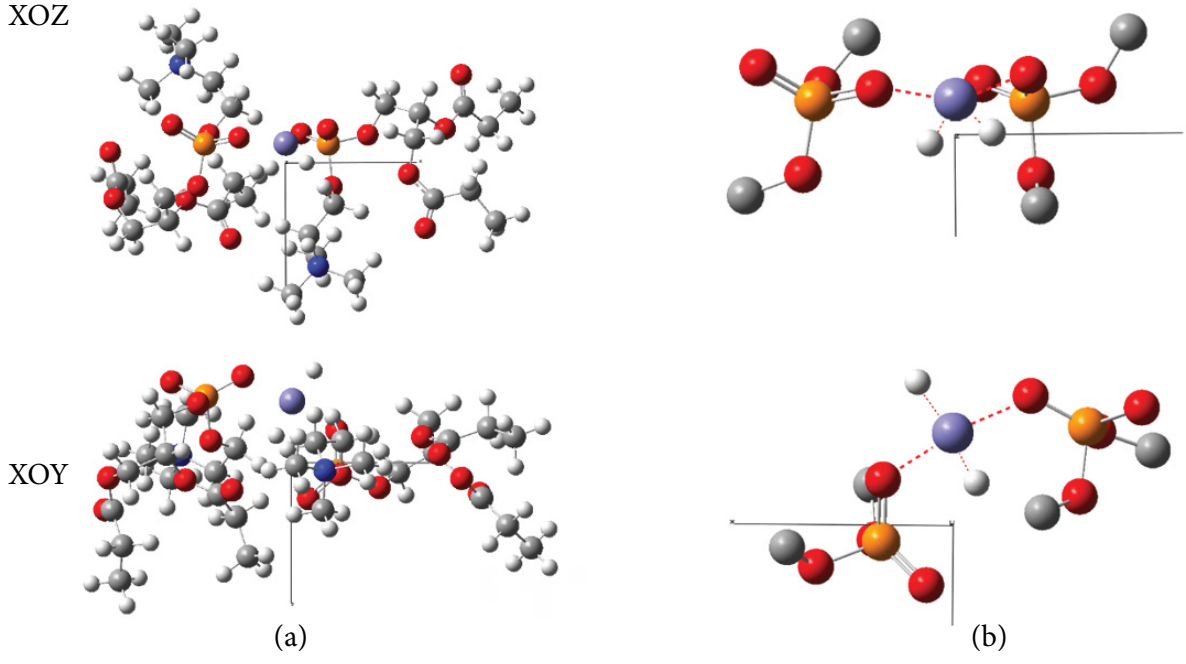

Fig. 9. D3 associate: two phospholipids related to the Fe^{2+} ion bridge in the orthophosphoric region (a) and the central region of bridge bonding (b). The top and bottom represent projections XOZ and XOY, respectively.

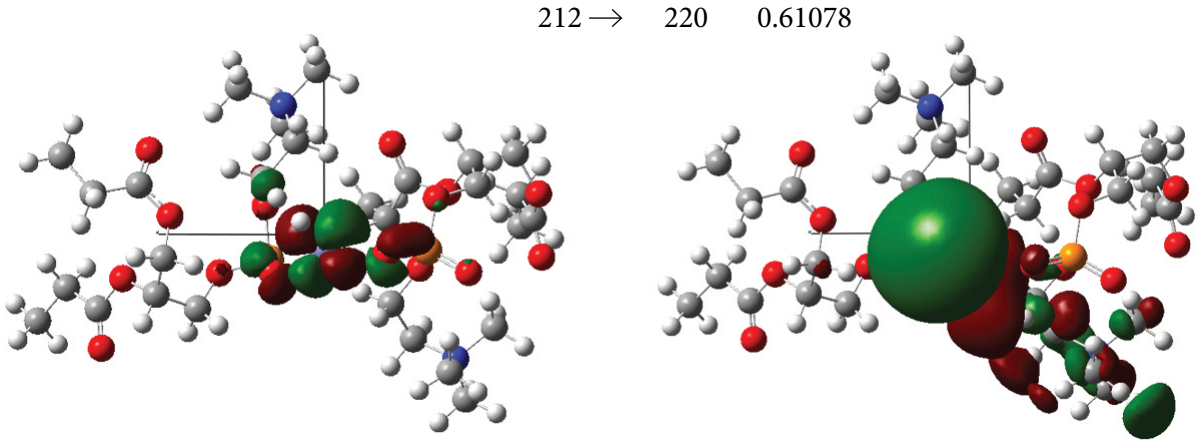

Fig. 10. D3 associate: two phospholipids bridged by Fe^{2+} ion in the orthophosphoric region, projection XOY. Molecular orbitals correspond to a forbidden electronic transition of 0.37 eV from the ground state (a) to the first excited state (b).

planar packing arrangement, consequently making pore closure less favourable once a defect has developed.

4. Discussion

This study focuses on a key unresolved aspect of electroporation: the persistence of membrane permeability for hours following electroporation, which significantly surpasses the closure times anticipated for solely electrostatic, water-filled pores [27, 28]. Through the application of solvated (PCM) B3LYP geometry optimizations and an analysis of low-lying excitations, we assessed the potential for redox-active metal ions and reactive oxygen species to (i) directly trigger chemical reactions at unsaturated chains or (ii) alternatively, stabilize lipid configurations that inhibit structural relaxation and pore closure.

A significant result is the spatial selectivity of metal–lipid coupling. Upon positioning Fe^{2+} (with hydroxyl anions/radicals) adjacent to the unsaturated aliphatic chain, the optimized structures revealed no occurrence of hydrogen abstraction, Fe^{2+} oxidation, or a significant tail rearrangement (Fig. 3). The current static models suggest that a direct initiation-like mechanism, where Fe^{2+}/ROS target the C=C-containing fragment to produce a lipid radical under these conditions, is not supported. Reactive oxygen species (ROS) are highly reactive structures formed as the products after interaction of any carbohydrates (in our case) with HOOH, HOH, and diatomic oxygen. This finding aligns with the wider experimental understanding that the effective iron-driven lipid peroxidation in membranes may necessitate the presence of pre-existing oxidized lipid species (LOOH/LOO•) to initiate chain reactions, rather than originating solely from intact lipids [51].

A head-group-proximal configuration (Fig. 4) was adopted following a chain-focused evaluation. The analysis revealed that positioning Fe^{2+} in the head-group region does not substantially affect the tail's conformation, supporting the decision to truncate the tail for more efficient optimization. The orthophosphate moiety serves as a strong binding site for metal coordination. Fe^{2+} readily forms lipid–Fe–lipid associates (D1–D3) via bridging interactions with the phosphoryl and non-bridging phosphate oxygens, resulting in stable head-group bonds with unique coordination geometries (Figs. 5, 7, 9) and a significant stabilization (Table 1). While it is probable that absolute binding energies are overestimated because of the simplified energy evaluation and the exclusion of solvent effects in those particular calculations [58], the qualitative outcome remains evident: metal binding at the orthophosphate interface is highly favoured and is associated with head-group reorientation and chain deformation – precisely the kind of packing frustration anticipated to initiate membrane defects.

This pathway is not exclusive to Fe^{2+}. Copper (Cu^{2+}), known for its role in metal-driven oxidative processes via the Haber–Weiss reaction, is often mentioned alongside iron as a key initiator

of lipid peroxidation chemistry [59, 60]. It is anticipated that it would interact with the oxygen-rich orthophosphate environment through robust O-donor coordination, considering that the availability of cellular metals is closely controlled and that only a limited labile pool is involved in redox reactions [45]. Localized or episodic enrichment of either Fe^{2+}/Fe^{3+} or Cu^{2+} at the membrane interface could facilitate the formation of similar metal-bridged head-group junctions. This establishes a shared structural pathway through which various redox-active metals can influence membranes to adopt defect-prone conformations, even before a significant chain oxidation occurs.

The analysis of excited states indicates potential pathways for these junctions to achieve longevity. The Fe^{2+}-bridged dimers display low-energy, forbidden charge-transfer transitions (D1: 0.79 eV; D2: 0.15 eV; D3: 0.37 eV; Figs. 6, 8, 10) that divide the complex into donor and acceptor lipids, redistributing charge toward the acceptor head group. This process frequently involves the $–NH_3$ moiety acting as a charge relay through a mixed $\sigma–\pi$ (and, in some instances, $n–\sigma–\pi$) character. One D2 excited-state configuration (MO 224) also interacts with the aliphatic tails, suggesting that metal bridging can make the chain regions more conducive to charge accommodation. Building on this principle, junctions containing Cu^{2+}, due to their unique electronic structure and redox flexibility, could potentially facilitate a similar (or enhanced) charge-transfer/charge-trapping behaviour at interfaces coordinated with phosphate, thus stabilizing distorted head-group geometries that resist bilayer relaxation.

The data collectively suggest a structural-electronic mechanism for the delayed resealing of membranes. The entry of metals such as Fe^{2+} and possibly Cu^{2+} into the orthophosphate region creates a head-group bridge, altering local packing. This is followed by donor–acceptor asymmetry and charge localization at the acceptor head group, which stabilizes the bridged state and hinders the restoration of a planar, tightly packed bilayer.

5. Conclusions

The modelling of phospholipid structures and their associations with iron ions through quantum molecular theory methods has shown that the binding of the metal ion to the lipid chain plays an insignificant role in the development of lipid conformational motion. No structural changes in conformation or energy were detected. In a similar manner, the fixation of metal ions is prohibited when it comes to the $[–NH_3]$ head within the lipid head group. A metal ion bridge was not formed between the two lipids $[–NH_3]$ in the head region.

The iron ion interacts with two lipid molecules in the orthophosphoric region, creating a stable connection between the orthophosphoric fragments. This process leads to a conformational transformation of the lipid aliphatic chains, forming a curved chain around the metal's centre rather than the original straight structure.

An analysis of molecular charge redistribution during excitation was conducted, focusing on the complex's structural asymmetry. Intermolecular charge redistribution and intramolecular charge were both acquired. The energetically favourable position of the Fe^{2+} ion results in one lipid acting as a charge donor while the other serves as a charge acceptor.

Acknowledgements

This work was supported by Grant S-MIP-20-29 from the Research Council of Lithuania (to GS). Computations were performed on resources at the High-Performance Computing Center 'HPC Sauletekis' in Vilnius University, Faculty of Physics.

References

[1] Y. Dai, H. Tang, and S. Pang, The crucial roles of phospholipids in aging and lifespan regulation, Front. Physiol. **12** (2021), https://doi.org/10.3389/fphys.2021.775648

[2] M. Pöhnl, M.F.W. Trollmann, and R.A. Böckmann, Nonuniversal impact of cholesterol on membranes mobility, curvature sensing and elasticity, Nat. Commun. **14** (2023), https://doi.org/10.1038/s41467-023-43892-x

[3] A.L. Santos and G. Preta, Lipids in the cell: Organisation regulates function, Cell. Mol. Life Sci. **75** (2018), https://doi.org/10.1007/s00018-018-2765-4

[4] R. Wardhan and P. Mudgal, Introduction to biomembranes, in: *Textbook of Membrane Biology*

(Springer Singapore, 2017) pp. 1–28, https://www.academia.edu/69731679/Textbook_of_Membrane_Biology

[5] P.L. Yeagle, Phospholipid headgroup behavior in biological assemblies, Acc. Chem. Res. **11** (1978), https://doi.org/10.1021/ar50129a001

[6] S. Mashaghi, T. Jadidi, G. Koenderink, and A. Mashaghi, Lipid nanotechnology, Int. J. Mol. Sci. **14** (2013), https://doi.org/10.3390/ijms14024242

[7] G. van Meer and A.I.P.M. de Kroon, Lipid map of the mammalian cell, J. Cell Sci. **124** (2011), https://doi.org/10.1242/jcs.071233

[8] D. Drabik, G. Chodaczek, S. Kraszewski, and M. Langner, Mechanical properties determination of DMPC, DPPC, DSPC, and HSPC solid-ordered bilayers, Langmuir **36** (2020), https://doi.org/10.1021/acs.langmuir.0c00475

[9] I. Schachter, R.O. Paananen, B. Fábián, P. Jurkiewicz, and M. Javanainen, The two faces of the liquid ordered phase, J. Phys. Chem. Lett. **13** (2022), https://doi.org/10.1021/acs.jpclett.1c03712

[10] R.X. Gu, S. Baoukina, and D.P. Tieleman, Phase separation in atomistic simulations of model membranes, J. Am. Chem. Soc. **142** (2020), https://doi.org/10.1021/jacs.9b11057

[11] D. Marsh, Structural and thermodynamic determinants of chain-melting transition temperatures for phospholipid and glycolipids membranes, Biochim. Biophys. Acta Biomembr. **1798** (2010), https://doi.org/10.1016/j.bbamem.2009.10.010

[12] S. Garcia-Manyes, G. Oncins, and F. Sanz, Effect of temperature on the nanomechanics of lipid bilayers studied by force spectroscopy, Biophys. J. **89** (2005), https://doi.org/10.1529/biophysj.105.065581

[13] H.J. Lessen, K.C. Sapp, A.H. Beaven, R. Ashkar, and A.J. Sodt, Molecular mechanisms of spontaneous curvature and softening in complex lipid bilayer mixtures, Biophys. J. **121** (2022), https://doi.org/10.1016/j.bpj.2022.07.036

[14] C. Sharma, P.V. Arya, and S. Singh, Lipid and membrane structures, in: *Introduction to Biomolecular Structure and Biophysics: Basics of Biophysics*, ed. G. Misra (Springer Singapore, 2017) pp. 139–182, https://doi.org/10.1007/978-981-10-4968-2_6

[15] T. Harayama and H. Riezman, Understanding the diversity of membrane lipid composition, Nat. Rev. Mol. Cell Biol. **19** (2018), https://doi.org/10.1038/nrm.2017.138

[16] A. Ayala, M.F. Muñoz, and S. Argüelles, Lipid peroxidation: Production, metabolism, and signaling mechanisms of malondialdehyde and 4-hydroxy-2-nonenal, Oxid. Med. Cell. Longev. **2014** (2014), https://doi.org/10.1155/2014/360438

[17] J.H. Choi and J.C. Kagan, Oxidized phospholipid damage signals as modulators of immunity, Open Biol. **15** (2025), https://doi.org/10.1098/rsob.240391

[18] A.J. Pereira, H. Xing, L.J. de Campos, M.A. Seleem, K.M.P. de Oliveira, S.K. Obaro, and M. Conda-Sheridan, Structure-activity relationship study to develop peptide amphiphiles as species-specific antimicrobials, Chem. Eur. J. **30** (2024), https://doi.org/10.1002/chem.202303986

[19] A. Ghorbel, F.M. André, L.M. Mir, and T. García-Sánchez, Electrophoresis-assisted accumulation of conductive nanoparticles for the enhancement of cell electropermeabilization, Bioelectrochemistry **137** (2021), https://doi.org/10.1016/j.bioelechem.2020.107642

[20] J.J. Sherba, S. Hogquist, H. Lin, J.W. Shan, D.I. Shreiber, and J.D. Zahn, The effects of electroporation buffer composition on cell viability and electro-transfection efficiency, Sci. Rep. **10** (2020), https://doi.org/10.1038/s41598-020-59790-x

[21] K. Qian, Y. Wang, Y. Lei, Q. Yang, and C. Yao, An experimental and theoretical study on cell swelling for osmotic imbalance induced by electroporation, Bioelectrochemistry **157** (2024), https://doi.org/10.1016/j.bioelechem.2023.108637

[22] S. Mahnič-Kalamiza and D. Miklavčič, The phenomenon of electroporation, in: *Pulsed Electric Fields Technology for the Food Industry*, Food Engineering Series (Springer Cham, 2022) pp. 107–141, https://doi.org/10.1007/978-3-030-70586-2_3

[23] J. Teissié, N. Eynard, B. Gabriel, and M.P. Rols, Electropermeabilization of cell membranes, Adv. Drug Deliv. Rev. **35** (1999), https://doi.org/10.1016/S0169-409X(98)00060-X

[24] M. Tarek, Membrane electroporation: A molecular dynamics simulation, Biophys. J. **88** (2005), https://doi.org/10.1529/biophysj.104.050617

[25] Y. Zhang, Z. Luo, and F. Guo, Simulation of electroporation threshold based on the evolution of transmembrane potential and pore density, PeerJ **13** (2025), https://doi.org/10.7717/peerj.19356

[26] D.P. Tieleman, The molecular basis of electroporation, BMC Biochem. **5** (2004), https://doi.org/10.1186/1471-2091-5-10

[27] L. Rems, M. Viano, M.A. Kasimova, D. Miklavčič, and M. Tarek, The contribution of lipid peroxidation to membrane permeability in electropermeabilization: A molecular dynamics study, Bioelectrochemistry **125** (2019), https://doi.org/10.1016/j.bioelechem.2018.07.018

[28] W.F.D. Bennett, N. Sapay, and D.P. Tieleman, Atomistic simulations of pore formation and closure in lipid bilayers, Biophys. J. **106** (2014), https://doi.org/10.1016/j.bpj.2013.11.4486

[29] M. Breton and L.M. Mir, Investigation of the chemical mechanisms involved in the electropulsation of membranes at the molecular level, Bioelectrochemistry **119** (2018), https://doi.org/10.1016/j.bioelechem.2017.09.005

[30] O.N. Pakhomova, V.A. Khorokhorina, A.M. Bowman, R. Rodaite-Riševičiene, G. Saulis, S. Xiao, and A.G. Pakhomov, Oxidative effects of nanosecond pulsed electric field exposure in cells and cell-free media, Arch. Biochem. Biophys. **527** (2012), https://doi.org/10.1016/j.abb.2012.08.004

[31] P.T. Vernier, Z.A. Levine, Y.H. Wu, V. Joubert, M.J. Ziegler, L.M. Mir, and D.P. Tieleman, Electroporating fields target oxidatively damaged areas in the cell membrane, PLoS One **4** (2009), https://doi.org/10.1371/journal.pone.0007966

[32] O. Yun, X.A. Zeng, C.S. Brennan, and Z. Han, Effect of pulsed electric field on membrane lipids and oxidative injury of *Salmonella typhimurium*. Int. J. Mol. Sci. **17** (2016), https://doi.org/10.3390/ijms17081374

[33] C. Tang, X. Qiu, Z. Cheng, and N. Jiao, Molecular oxygen-mediated oxygenation reactions involving radicals, Chem. Soc. Rev. **50** (2021), https://doi.org/10.1039/D1CS00242B

[34] K.J.A. Davies, Oxidative stress, antioxidant defenses, and damage removal, repair, and replacement systems, IUBMB Life **50** (2000), https://doi.org/10.1080/713803728

[35] A. Rahal, A. Kumar, V. Singh, B. Yadav, R. Tiwari, S. Chakraborty, and K. Dhama, Oxidative stress, prooxidants, and antioxidants: The interplay, Biomed. Res. Int. **2014** (2014), https://doi.org/10.1155/2014/761264

[36] L. Valgimigli, Lipid peroxidation and antioxidant protection, Biomolecules **13** (2023), https://doi.org/10.3390/biom13091291

[37] A. Catalá and M. Díaz, Editorial: Impact of lipid peroxidation on the physiology and pathophysiology of cell membranes, Front. Physiol. **7** (2016), https://doi.org/10.3389/fphys.2016.00423

[38] J. Wong-Ekkabut, Z. Xu, W. Triampo, I.M. Tang, D.P. Tieleman, and L. Monticelli, Effect of lipid peroxidation on the properties of lipid bilayers: A molecular dynamics study, Biophys. J. **93** (2007), https://doi.org/10.1529/biophysj.107.112565

[39] E. Niki, Y. Yoshida, Y. Saito, and N. Noguchi, Lipid peroxidation: Mechanisms, inhibition, and biological effects, Biochem. Biophys. Res. Commun. **338** (2005), https://doi.org/10.1016/j.bbrc.2005.08.072

[40] S. Sasson, Nutrient overload, lipid peroxidation and pancreatic beta cell function, Free Radic. Biol. Med. **111** (2017), https://doi.org/10.1016/j.freeradbiomed.2016.09.003

[41] M.M. Gaschler and B.R. Stockwell, Lipid peroxidation in cell death, Biochem. Biophys. Res. Commun. **482** (2017), https://doi.org/10.1016/j.bbrc.2016.10.086

[42] H. Yin, L. Xu, and N.A. Porter, Free radical lipid peroxidation: Mechanisms and analysis, Chem. Rev. **111** (2011), https://doi.org/10.1021/cr200084z

[43] N.A. Porter, Mechanisms for the autoxidation of polyunsaturated lipids, Acc. Chem. Res. **19** (1986), https://doi.org/10.1021/ar00129a001

[44] D.A. Pratt, K.A. Tallman, and N.A. Porter, Free radical oxidation of polyunsaturated lipids: New mechanistic insights and the development of

peroxyl radical clocks, Acc. Chem. Res. **44** (2011), https://doi.org/10.1021/ar200024c

[45] E. Gammella, S. Recalcati, I. Rybinska, P. Buratti, and G. Cairo, Iron-induced damage in cardiomyopathy: Oxidative-dependent and independent mechanisms, Oxid. Med. Cell Longevi (2015), https://doi.org/10.1155/2015/230182

[46] M. Hayyan, M.A. Hashim, and I.M. Alnashef, Superoxide ion: Generation and chemical implications, Chem. Rev. **116** (2016), https://doi.org/10.1021/acs.chemrev.5b00407

[47] H.J.H. Fenton, LXXIII. – Oxidation of tartaric acid in presence of iron, J. Chem. Soc. Transact. **65** (1894), https://doi.org/10.1039/CT8946500899

[48] S. Lewis, V. Smuleac, A. Montague, L. Bachas, and D. Bhattacharyya, Iron-functionalized membranes for nanoparticle synthesis and reactions, Sep. Sci. Technol. **44** (2009), https://doi.org/10.1080/01496390903212805

[49] R.F. Castilho, A.R. Meinicke, A.E. Vercesi, and M. Hermes-Lima, Role of Fe(III) in Fe(II)Citrate-mediated peroxidation of mitochondrial membrane lipids, Mol. Cell Biochem. **196** (1999), https://doi.org/10.1023/A:1006988129221

[50] K. Yoshida, J. Terao, T. Suzuki, and K. Takama, Inhibitory effect of phosphatidylserine on iron-dependent lipid peroxidation, Biochem. Biophys. Res. Commun. **179** (1991), https://doi.org/10.1016/0006-291X(91)91929-7

[51] L. Tang, Y. Zhang, Z. Qian, and X. Shen, The mechanism of Fe^{2+}-initiated lipid peroxidation in liposomes: The dual function of ferrous ions, the roles of the pre-existing lipid peroxides and the lipid peroxyl radical, Biochem. J. **352** (2000), https://doi.org/10.1042/bj3520027

[52] F.J. Schopfer, C. Cipollina, and B.A. Freeman, Formation and signaling actions of electrophilic lipids, Chem. Rev. **111** (2011), https://doi.org/10.1021/cr200131e

[53] A. Higdon, A.R. Diers, J.Y. Oh, A. Landar, and V.M. Darley-Usmar, Cell signalling by reactive lipid species: New concepts and molecular mechanisms, Biochem. J. **442** (2012), https://doi.org/10.1042/BJ20111752

[54] K. Vanommeslaeghe, O. Guvench, and A.D. MacKerell Jr, Molecular mechanics, in: *Catalysis from A to Z: A Concise Encyclopedia* (Wiley, 2013).

[55] A. Gruodis, *Liuminescencija* (Biznio mašinų kompanija, Vilnius, 2008).

[56] M.J. Frisch, G.W. Trucks, H.B. Schlegel, G.E. Scuseria, M.A. Robb, J.R. Cheeseman, G. Scalmani, V. Barone, G.A. Petersson, H. Nakatsuji, et al., *Gaussian 16* (2016).

[57] G. Scalmani and M.J. Frisch, Continuous surface charge polarizable continuum models of solvation. I. General formalism, J. Chem. Phys. **132** (2010), https://doi.org/10.1063/1.3359469

[58] M.C. Durrant, A computational study of ligand binding affinities in Iron(Iii) porphine and protoporphyrin IX complexes, Dalton Trans. **43** (2014), https://doi.org/10.1039/c4dt01103a

[59] J. Pincemail, E. Cavalier, C. Charlier, J.P. Cheramybien, E. Brevers, A. Courtois, M. Fadeur, S. Meziane, C. Le Goff, B. Misset, et al. Oxidative stress status in COVID-19 patients hospitalized in intensive care unit for severe pneumonia. A pilot study, Antioxidants **10** (2021), https://doi.org/10.3390/antiox10020257

[60] F. Elgendey, R.A. Al Wakeel, S.A. Hemeda, A.M. Elshwash, S.E. Fadl, A.M. Abdelazim, M. Alhujaily, and O.A. Khalifa, Selenium and/or vitamin E upregulate the antioxidant gene expression and parameters in broilers, BMC Vet. Res. **18** (2022), https://doi.org/10.1186/s12917-022-03411-4

Fe^{2+} ĮTAKA LIPIDŲ ORIENTACIJAI LĄSTELĖS MEMBRANOS DVISLUOKSNYJE: MODELIAVIMAI KVANTINĖS CHEMIJOS METODAIS

T. Kondrotaitė-Intė [a, b], A. Gruodis [c], G. Saulis [b]

[a] *Vilniaus Gedimino technikos universiteto Mechanikos ir medžiagų inžinerijos katedra, Vilnius, Lietuva*

[b] *Vytauto Didžiojo universiteto Gamtos mokslų fakulteto Biologijos katedra, Akademija, Kaunas, Lietuva*

[c] *Vilniaus universiteto Cheminės fizikos institutas, Vilnius, Lietuva*

Santrauka

Siekiant suprasti ląstelės membranos skyles formuojančių procesų dinamiką ir skylės užsidarymo progresavimą sluoksnyje žemiausiu molekuliniu lygmeniu, buvo atliktas fosfolipidų ir geležies jonų asociatų struktūros modeliavimas kvantinės molekulinės teorijos metodais. Nustatyta, kad metalo jonų fiksavimasis prie lipidų grandinės nevyksta. Panašiai, metalo jono prisijungimas prie lipidų galvos grupės $–N(CH_3)_3$ yra neįmanomas. Geležies jonas jungia dviejų lipidų molekulės ortofosforo fragmentus, taip sudarydamas energetiškai stabilų tiltą. Šio proceso rezultatas – lipidų alifatinės grandinės keičia konformaciją – iš tiesios struktūros susiformuoja lenkta grandinė link metalo jono. Buvo nustatytas ir aprašytas tipiškas molekulinio krūvio persiskirstymas įvykstant sužadinimui. Teigiama, kad dėl energetiškai palankios Fe^{2+} jono padėties viena lipidų molekulė tampa krūvio donoru, o kita – krūvio akceptoriumi.